Langmuir

Article

pubs.acs.org/Langmuir

Supramolecular Structure of Self-Assembled Monolayers of Ferrocenyl Terminated *n*-Alkanethiolates on Gold Surfaces

Nisachol Nerngchamnong,[†] Hairong Wu,[‡] Kai Sotthewes,[‡] Li Yuan,[†] Liang Cao,[†] Max Roemer,[†] Jiong Lu,[†] Kian Ping Loh,[†,∥] Cedric Troadec,[§] Harold J. W. Zandvliet,[‡] and Christian A. Nijhuis*[,†,∥]

[†]Department of Chemistry, National University of Singapore, 3 Science Drive 3, Singapore 117543

[‡]Physics of Interfaces and Nanomaterials, MESA+ Institute for Nanotechnology, University of Twente, 7500 AE Enschede, The Netherlands

[§]Institute of Materials Research and Engineering, 3 Research Link, Singapore 117602

[∥]Graphene Research Centre, National University of Singapore, 6 Science Drive 2, Singapore 117546

Supporting Information

ABSTRACT: It is important to understand the structure of redox-active self-assembled monolayers (SAMs) down to the atomic scale, since these SAMS are widely used as model systems in studies of mechanisms of charge transport or to realize electronic functionality in molecular electronic devices. We studied the supramolecular structure of SAMs of *n*-alkanethiolates with ferrocenyl (Fc) end groups ($S(CH_2)_nFc$, n = 3 or 4) on Au(111) by scanning tunneling microscopy (STM). In this system, the tilt angle of the Fc units with respect to the surface normal (α) depends on the value of n because the Au−S−C bond angle is fixed. The ordered domains of the SAMs were imaged by STM after annealing at 70 °C at ultrahigh vacuum conditions. High resolution electron energy loss spectroscopy (HREELS) and cyclic voltammetry show that this annealing step only removed physisorbed material and did not affect the structure of the SAM. The STM images revealed the presence of row defects at intervals of 4 nm, that is, six molecules. We determined by near edge X-ray absorption fine structure spectroscopy (NEXAFS) that the Fc units of the SAMs of SC_3Fc are more parallel to the Au(111) plane with a tilt angle α = 60.2° than the Fc units of SC_4Fc SAMs (α = 45.4°). These tilt angles are remarkably close to the tilt angles measured by X-ray diffraction data of bulk crystals (*bc*-plane). Based on our data, we conclude that the molecules are standing up and the SAMs pack into lattices that are distorted from their bulk crystal structures (because of the build-up stain due to the differences in size between the Fc units and thiolate anchoring groups).

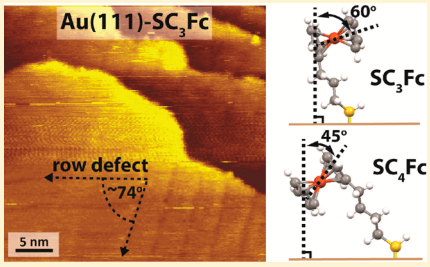

INTRODUCTION

Redox-active self-assembled monolayers (SAMs) have been widely applied in molecular/organic electronics,[1,2] in energy storage,[3] in photovoltaics,[4] in biomolecular systems,[5] and as model systems to investigate the mechanisms of charge transport through molecules and their interfaces with the electrodes and/or electrolyte. The supramolecular structures of the SAMs are important to understand in physical-organic studies involving charge transport but are often not well-understood.[6,7] For instance, the electrochemical behavior of SAMs of ferrocenyl-alkanethiolates ($S(CH_2)_nFc$ abbreviated as SC_nFc) have been widely studied because of the good electrochemical stability, and synthetic flexibility,[8] since the early 1990s,[9−11] but their electrochemical behavior is still not completely understood. We showed that subtle changes in the supramolecular structures of these SAMs incorporated in SAM-based tunnel junctions have a large influence on the electrical properties of the junctions by just changing the length of the carbon backbone (n) from even (n_{even}) to odd (n_{odd}) numbered.[12] These so-called odd−even effects have been observed for other types of SAMs as well and affect melting points, electron transfer rates, or stabilities against radiation damage.[13] Here we propose three-dimensional (3D) models for SAMs of SC_nFc on Au(111) with n = 3 and 4 based on a combination of complementary characterization techniques. We believe that these models are useful for future studies of charge transport through these SAMs, and they provide insightful information on, for instance, understanding odd−even effects.

Most surface characterization techniques provide often only qualitative information regarding a certain aspect of the SAM over a large area, whereas scanning probe based techniques yield detailed real space images, but only probe a small fraction of the surface.[14−17] Often it is difficult to reconcile data obtained by, for instance, scanning probe methods with other techniques because it is not always clear whether the image (small) area is representative for the whole surface. Techniques that sample large areas on surfaces only yield spatially averaged data and, for instance, inhomogeneous surfaces or the presence of different phases, hamper the interpretation of the data. For

Received: September 3, 2014
Revised: October 16, 2014
Published: October 17, 2014

   dx.doi.org/10.1021/la503493x | Langmuir 2014, 30, 13447−13455

example, mixed SAMs of SC_nFc with *n*-alkanethiolates, SC_n, suffer from phase separation,[18] leading to nonuniform surface properties at the nanometer scale. The structures of pure SAMs of SC_nFc have rarely been characterized by scanning tunneling microscopy (STM),[19,20] but these SAMs are used in various applications including electrochemical switches,[21] memories,[22] electronic gates,[23] and diodes;[24] therefore, it is important to understand their structures at the atomistic scale.

Previously, we[12] reported that small changes in the packing of the SAMs can have a profound effect on the charge transport properties across them in molecular tunnel junctions of the form Ag^{TS}-SC_nFc//GaO_x/EGaIn (where Ag^{TS} denotes a template-stripped silver surface, and the GaO_x/EGaIn is the top-electrode of a non-Newtonian liquid-metal alloy of Ga and In with a thin (0.7 nm) conductive surface layer of GaO_x).[25] These junctions are molecular diodes with rectification ratios of 1.0×10^2 but only when n_{odd} is in the range of $n = 7-15$. For junctions with n_{even}, the rectification ratios drops by a factor of 10, the reproducibility by a factor of 2−3, and the yield by about 10%. The number of CH_2 units in the backbone of the SAM determines the orientation of the Fc units with respect to the surface normal, that is, the so-called tilt angle α (deg). The tilt angle is determined by *n*: for SAMs formed on Au, the Fc units in SAMs with n_{even} stand up more (the value of α is smaller) than the Fc units in SAMs with n_{odd}. Therefore, the alkyl chains in SAMs with n_{even} pack better by 0.5 kcal/mol than SAMs with n_{odd}; this difference in the packing energy caused the observed odd−even effects.[12] In addition, these SAMs also showed odd−even effects in their electrochemical behavior, which we related to the packing energy: SAMs with n_{even} pack better than SAMs with n_{odd} and are therefore more difficult to oxidize (by ∼25 meV). For these reasons, we believe SC_nFc SAMs (with $n = 3$ or 4) are good model systems to study odd−even effects at the nanoscale by STM.

The packing of the SAMs is driven by the nature of sulfur−gold bond and intermolecular interactions[26,27] and, more specifically for this work, alkyl−alkyl chain, Fc−alkyl chain, and Fc−Fc interactions. It is well-known that the structure of SAMs of SC_n on Au(111) is $(\sqrt{3} \times \sqrt{3})$ *R*30°.[28,29] Replacing the CH_3 terminus by bulkier groups (SC_nX, X = OH, COOH, NH_2, phenyl, or ferrocene, for instance) hampers ideal packing of the alkyl chains and causes deviations from the $(\sqrt{3} \times \sqrt{3})$ *R*30° packing, increases the number of defects, and reduces the domain size.[27,30] To minimize steric hindrance between the terminal groups, and to obtain well-ordered structures, mixed SAMs on Au composed of SC_nFc and SC_n have been studied by STM.[31−33] In addition, physisorbed Fc functionalized monolayers on highly ordered pyrolytic graphite (HOPG) have been investigated by STM.[34,35]

Pure SAMs of SC_nFc have occasionally been characterized by STM. Rudnev et al.[36] reported that for SAMs of SC_nCOFc with short alkyl chains ($n = 4, 6, 8$) it was difficult to observe ordered domains, because of a liquidlike behavior of the short alkyl chains due to weak alkyl−alkyl chain interactions.[37] Others reported that annealing at 70 °C resulted in relatively well-ordered surfaces that were suitable for STM investigations.[38,39] These authors did not provide any information regarding whether annealing improves the packing of the SAMs or merely removes loosely bound molecules from the surface. Here we studied the difference in packing of SAMs of SC_nFc with $n = 3$ and 4 on Au(111) by STM. We found that annealing the SAMs in ultrahigh vacuum removes physisorbed materials; this annealing step does not induce conformational changes neither does it cause damage to the SAMs. We compared the packing of the SAMs on Au(111) to the packing of the molecules in macroscopic crystals which were determined by single crystal X-ray diffraction (XRD). We observed that the SAMs packed well with structures similar to that of the bulk crystals, but the structures are distorted because of the mismatch in sizes between the sulfur atoms, Au atoms, and the Fc units. This mismatch induced strain that caused so-called row defects at intervals of six molecules. The Au−S−C bond angle is fixed at 109.5°, and therefore, the number of CH_2 units determines the value of α.[13,27,40] The experimental values of α in SAMs (determined by near edge X-ray adsorption spectroscopy, NEXAFS) match very well to those extracted from the bulk crystal structures (see below for details) from which we conclude that the SAMs form dense layers with similar structures in a bulk crystal. Based on these data, we conclude that the real space STM images represent the SAMs very well and we propose models for the SAM that help to understand the experimentally observed odd−even effects.

EXPERIMENTAL SECTION

Preparation of the Au Substrates. The hydrogen flame annealed and template stripped (TS) Au substrates were prepared following reported procedures[41] (Supporting Information page S2). The hydrogen flame annealed Au substrates were used for the STM measurements, and Au^{TS} substrates were used for high resolution electron energy loss spectroscopy (HREELS), cyclic voltammetry, and NEXAFS.

Preparation of the Self-Assembled Monolayers. We synthesized the HSC_nFc ($n = 3, 4$) compounds following previously reported procedures.[42] The Au substrates were immersed into the corresponding ethanolic solutions of 2−3 mM of HSC_nFc immediately after fabrication. We formed the SAMs over a period of time of 3−5 h. The samples were thoroughly rinsed with absolute ethanol, blown to dryness in a stream of pure N_2 gas, and used immediately.

Scanning Tunneling Microscopy. We performed the STM measurements using a RHK UHV700 system at room temperature under ultrahigh vacuum (UHV) conditions (2.0×10^{-10} mbar). We used electrochemically etched tungsten tips. We annealed the SAMs at ∼70 °C for 45 min in UHV before we started the measurements. The STM images were recorded at a sample bias range of ±1 to ±2 V with a range of tunneling currents of 30−100 pA.

High Resolution Electron Energy Loss Spectroscopy. The HREELS measurements were performed in a dual-chamber UHV system equipped with a Delta 0.5 high resolution electron energy loss spectrometer with a mu-metal magnetic shield. The sample stage was kept at the desired temperature within ±1 °C at a base pressure of 2.0×10^{-10} mbar. The specular spectra ($\theta_{inc} = 53°$) were taken with an incident electron beam of 5 eV. We annealed the SAMs at the desired temperatures for 60 min and recorded spectra before and after annealing.

Near Edge X-ray Absorption Fine Structure Spectroscopy. The NEXAFS data were recorded using the SINS (Surface, Interface and Nanostructure Science) beamline of the Singapore Synchrotron Light Source (SSLS) in an UHV chamber with a base pressure of 1×10^{-10} mbar. We collected the angular dependent C *K*-edge NEXAFS spectra in Auger electron yield (AEY) mode and a Scienta R4000 electron energy analyzer. We used two different angles to determine the molecular orientations: normal incidence (90°) and grazing incidence 20° (Supporting Information page S2).

Cyclic Voltammetry. The cyclic voltammograms (CVs) were recorded using an Autolab PGSTAT302N potentiostat (Metrohm) and Nova 1.10 software. We used a custom built electrochemical cell equipped with a platinum counter electrode and a Ag/AgCl reference electrode, and the Au^{TS} served as a working electrode. CVs were recorded in an aqueous solution of 1.0 M $HClO_4$, between −0.1 and 0.9 V at a scan rate of 1.0 V/s.

dx.doi.org/10.1021/la503493x | *Langmuir* 2014, 30, 13447−13455

X-ray Single Crystal Diffraction. The crystal structures of HSC_3Fc (CCDC no.: 1020652) and HSC_4Fc (CCDC no.: 1020653) were determined using Bruker Apex2 and SMART diffractometers. Single crystals of HSC_3Fc and HSC_4Fc were grown from solutions of pentane at −20 °C, and the crystals were selected using an optical microscope equipped with a polarization filter. Structures were solved by direct methods using SHELXS-97 software.[43] The crystallographic data are given in the Supporting Information page S4. We determined the value of α with respect to the surface normal of the *bc*-plane of the crystal structure.

RESULTS AND DISCUSSION

Characterization of the SAMs before and after Annealing. We found that physisorbed materials were always present on the SAMs despite rinsing with excess amounts of solvents. These physisorbed materials are generally composed of water and organic molecules (their composition depends on the environmental conditions), and residual HSC_nFc. Others have reported that SAMs of SC_8 are stable in UHV conditions up to a temperature of 120 °C.[39,44] To remove the physisorbed materials, we annealed the SAMs in UHV (2.0×10^{-10} mbar) for 45 min at 70 °C (see below). To prove that during annealing the SAMs were not damaged or altered in other ways, we followed the annealing process by HREELS. Figure 1A shows the HREELS data for the SC_3Fc SAM before annealing. We assigned nine peaks (labeled P_1−P_9) that are listed in Table 1 following previously reported assignments.[45−47] The signals labeled P_1, P_3, P_4, P_6, P_7, and P_9 are the vibrational modes of the Fc moieties, and P_5 and P_8 are vibrational modes of the alkyl chains. The intensities of P_3 and P_4 display a strong angular dependence where the angle is measured between the surface normal and π molecular orbital vector (the cyclopentadienyl, or the Cp ring plane) because of the dipole selection rule (only vibrational modes can be detected when the change in dipole moment is perpendicular to the surface). The relative intensities of these signals give information regarding the value α of the Fc unit. Here, the intensity of P_3 is lower than that of P_4 for SC_3Fc SAMs, which indicates that the out of plane C−H bending (P_3) modes are more perpendicular to the surface normal than the P_4 bending mode (which is in plane of the ring). To confirm our peak assignments and interpretation of the spectra, we also recorded HREEL spectra of SC_4Fc after annealing (Figure 1C). The relative intensities of P_3 and P_4 are reversed for the SC_4Fc SAM, indicating that its Fc units are more parallel orientated with respect to the surface normal than the Fc units of the SC_3Fc SAM. These data agree with the more accurately determined α values by NEXAFS (see below).

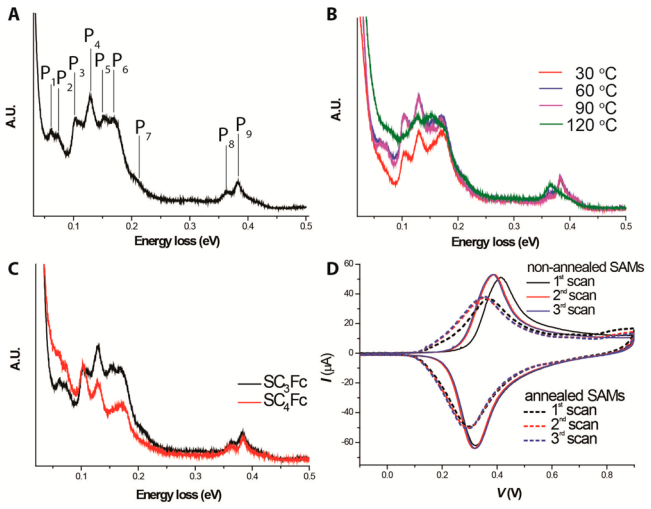

Figure 1. (A) HREEL spectrum of a SC_3Fc SAM on Au^{TS}; peak assignments are listed in Table 1. (B) HREEL spectra of a SC_3Fc SAM annealed for 1 h at 30 °C (red line), 60 °C (blue line), 90 °C (purple line), and 120 °C (green line). (C) HREEL spectra of a SAM of SC_3Fc (black line) and SC_4Fc (red line) on Au^{TS} annealed at 90 °C for 1 h. (D) CVs of nonannealed (solid line) and annealed (dashed line) SC_3Fc SAMs, 10 scans recorded at a scan rate of 1.0 V/s with aqueous 1.0 M $HClO_4$ as the electrolyte and a Ag/AgCl reference electrode.

Figure 1B shows the HREEL spectra of the SAMs of SC_3Fc on Au^{TS} after annealing at four different temperatures in high vacuum (10^{-7} mbar) for 1 h at 30, 60, 90, and 120 °C. These results show that the spectra did not change after annealing up to 90 °C apart from an increase of the signal-to-noise ratio from which we conclude that the SAMs were stable and did not change during the experiment, and that physisorbed molecules were removed from the surface. In contrast, the spectrum recorded after annealing at 120 °C changed significantly. Peak P_3 vanished, and the intensity of P_4 decreased, indicating that the surface coverage decreased and that the remaining molecules lie flat on the surface (with the Cp rings perpendicular to the surface normal). The intensities of P_5 and P_8 increased while those of P_6 and P_9 decreased which agree with an increase of exposure of the alkyl chains consistent for flat-lying molecules. These results indicate that the SAMs decomposed and the molecules desorbed from the surface at 120 °C.

We also characterized the SAMs by cyclic voltammetry with aqueous 1 M $HClO_4$ as the electrolyte. Figure 1D shows the CVs before and after annealing of the SAMs of SC_3Fc at 70 °C for 1 h in vacuum (10^{-7} mbar). The difference between the first and second scan is more pronounced for the nonannealed surfaces than that for the annealed surfaces. It is well-known that the Fc units in their oxidized state have a higher solubility in water than the Fc units in its neutral form.[48] During the first scan, the Fc units convert to Fc^+ and the physisorbed molecules desorb from the surface and dissolve in the electrolyte. The shape of the CVs did not change during the nine consecutive scans. From this experiment, we conclude that the SAMs are, as expected, stable under our electrochemical conditions and that during the experiment only physisorbed material was removed from the SAM.

Surface Coverage. We determined the surface coverage of the Fc units, Γ_{Fc} (mol/cm^2), from the CVs. The Γ_{Fc} can be calculated by using eq 1, where Q_{tot} is the total charge obtained by integration of the CV, n is the number of electrons per mole of reaction, F is the Faraday constant, and A is the surface area of the electrode exposed to the electrolyte solution (0.33 cm^2).

$$\Gamma_{Fc} = Q_{tot}/nFA \quad (1)$$

The surface coverage of the nonannealed SAMs ($2.98 \pm 0.14 \times 10^{-10}$ mol/cm^2) is slightly higher than that of the annealed SAMs ($2.81 \pm 0.02 \times 10^{-10}$ mol/cm^2). Here the error bars represent the standard deviation of three experiments, but in each experiment the surface coverage was higher before than after annealing. We observed that, after annealing, the CVs became slightly broader (the full width at half-maximum increased by 63 ± 2 mV) which may indicate improved interactions between the Fc units in the SAMs.[49] Additionally, the peak oxidation potential shifted to more negative potentials by 22 ± 2 mV, indicating that SAMs tend to be oxidized more

dx.doi.org/10.1021/la503493x | Langmuir 2014, 30, 13447−13455

Table 1. Peak Assignments for HREEL In-Specular Direction Spectra of the SAMs of SC_3Fc and SC_4Fc on Au^{TS} before and after Annealing

peak	peak position (meV)	ref	peak position before annealing (meV) (this work)		peak position after annealing[b] (meV) (this work)		peak assignments
			SC_3Fc	SC_4Fc	SC_3Fc	SC_4Fc	
P_1	60	45	none[a]	none[a]	59	55	
P_1	59.3	46					antisymmetric iron-ring stretch
P_1	53.8	47					
P_2	79.1	47	none[a]	none[a]	72	69	E_{2g}, π(CH)
P_3	100.5	45	101	101	101	101	
P_3	102	46					C−H bend out of the plane of the rings: A_{2u}, π(CH)
P_3	108.6	47					
P_4	130.2	45	130	130	130	129	
P_4	125	46					C−H bend in the plane of the rings: E_{1u}, π(CH)
P_4	115.8	47					
P_5	155.5	45	153	153	153	153	A_{2u}, δ(CH)
P_5	148.4	47					
P_6	178.6	45	170	169	170	169	
P_6	175	46					E_{2u}, π(CH)
P_6	182.8	47					
P_7	199.3	45	211	210	211	210	
P_7	210	46					E_{1u}, π(CH)
P_7	196.0	47					
P_8	363.3	45	363	360	363	360	V(C−H) sp^3
P_9	382.4	45	383	383	383	383	V(C−H) sp^2
P_9	386	46					

[a] P_1 and P_2 are very close to the noise levels before annealing, and therefore, their peak positions could not be determined. [b] The surfaces were annealed at 90 °C for 1 h in ultrahigh vacuum (2.0×10^{-10} mbar).

easily, which agrees with the removal of physisorbed materials. Although these changes in the CV data are small, the CV results are in agreement with the HREELS data and annealing at 70 °C for 1 h in vacuum removes most of the physisorbed materials. The CV data seem to suggest that SAM packing improved slightly during annealing, but any changes in the HREEL spectra were not apparent. Therefore we believe that annealing did not induce any conformational changes or phase transitions, or alter the surface coverage.

Tilt Angles of the Fc Units. We determined the α values by NEXAFS. Figure 2A shows the angular dependent NEXAFS at the C *K*-edge for SAMs of SC_3Fc and SC_4Fc on Au^{TS}. The signals 1 and 2 are assigned to the transitions from C 1*s* to π^* orbitals ($4e_{1g}$ at 285.4 eV and $3e_{2u}$ at 286.9 eV) associated with the Cp rings of ferrocene.[50] The vectors of the π^* orbitals are perpendicular to the Cp plane. The value of α was determined by monitoring the changes in intensities of peaks 1 or 2 as a function of the incidence angle of the X-ray beam following previously reported procedures (see Supporting Information for more details).[51,52] The α values are 60.2° for the SC_3Fc SAMs and 45.4° for the SC_4Fc SAMs.

Figure 2B shows the CV graphs of SAMs of SC_3Fc and SC_4Fc. The CV data show that the peak oxidation potential of SAMs of SC_3Fc (401 ± 11 mV) is higher than that of SAMs of SC_4Fc (363 ± 3 mV), by 38 ± 14 mV. A higher anodic peak potential (more difficult to oxidize) may be caused by higher packing energy, or stronger Fc−Fc interactions, since oxidation of Fc to Fc^+ ion and the strong interaction between Fc^+ and ClO_4^- ions causes rearrangements of the supramolecular structures of SAMs.[53] Therefore, we believe that, in SAMs of SC_3Fc, the Fc units interact stronger with each other by 38 ± 13 mV (0.88 ± 0.032 kcal/mol) than those in SAMs of SC_4Fc.

Packing in the Solid State. Although the bulk and surface packing structures are difficult to compare to each other due to different driving forces for bulk packing (intermolecular interactions) and surface packing (intermolecular interactions and molecule−surface interactions), we show below that bulk crystal structures are helpful and support our models since the packing structure of the SAMs with short chains ($n = 3 - 4$) is largely driven by Fc−Fc interactions because of the short length of the alkyl chains and the associated weak van der Waals interactions between them (see Supporting Information page S5 for the crystal structures and a more detailed discussion). We determined the tilt angle α of the Fc units with respect to the surface normal that is perpendicular to a surface plane (*bc*-plane; the thiol moieties lie in one plane) of the crystal packing of HSC_3Fc and HSC_4Fc using the Mercury program.[54] We obtained values of α = 61.55° and 44.06° for HSC_3Fc and HSC_4Fc, respectively (see Table 2).

Unfortunately, the orientation of Fc group in the SAMs could not be extracted from the available real space images as obtained by STM (see below). From the NEXAFS data, we derived α = 60.2° and 45.4° for SAMs of SC_3Fc and SC_4Fc, respectively[55] (Figure 2A), which is in quantitative agreement with the XRD data (α = 61.55° and 44.06° for HSC_3Fc and HSC_4Fc, respectively). These values are also in qualitative agreement with the HREELS data (Figure 1C). The more horizontal orientation of Fc groups of the SC_3Fc SAMs (~15° larger α values) possibly induces edge-to-face (EF) interactions, which is similar to the arrangement in the known monoclinic and orthorhombic forms of native ferrocene (determined by single crystal XRD).[56,57] The more favorable EF interactions among the Fc groups leads to stronger lateral interactions and higher packing density, resulting in an increase in the value of

dx.doi.org/10.1021/la503493x | *Langmuir* 2014, 30, 13447−13455

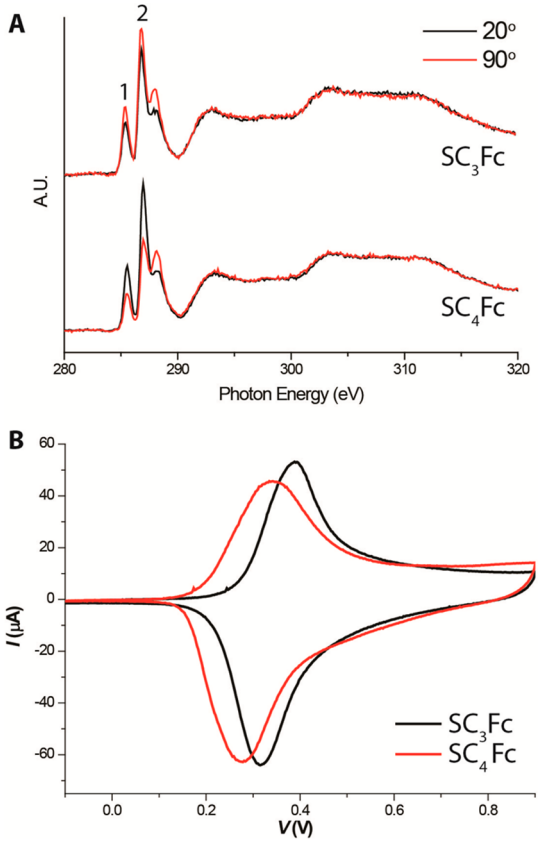

Figure 2. (A) NEXAFS spectra for SAMs of SC_3Fc and SC_4Fc recorded at the incident angle (90°) and a grazing angle (20°). Peaks 1 and 2 are assigned to the transitions from C 1s to π^* orbitals ($4e_{1g}$ at 285.4 eV and $3e_{2u}$ at 286.9 eV) associated with the Cp rings. (B) CV graphs of the SAMs of SC_3Fc and SC_4Fc on Au^{TS} at scan rate of 1.0 V/s, with aqueous 1.0 M $HClO_4$ as the electrolyte and a Ag/AgCl reference electrode.

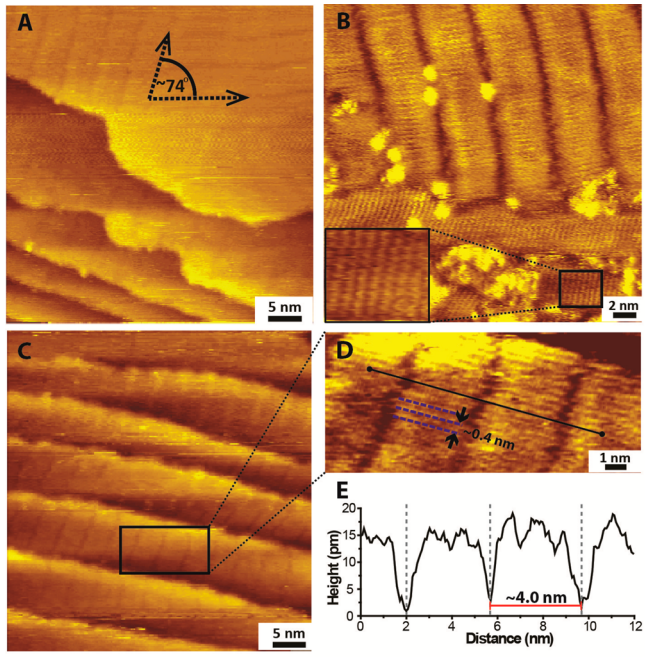

Figure 3. (A) STM images of well-ordered domains of SAMs of SC_3Fc on Au(111) showing the different domains. (B) Magnification of the stripes with a width of ~4 nm. The stripes exhibit a fine periodicity of ~0.4 nm along the defect row direction. (C) Domains of well-ordered stripes of ~4 nm width extending over step edges. (D) Magnification of the pattern in panel (C) showing the periodicity of ~0.4 nm marked in blue. (E) STM height profile recorded along the solid black line in panel (D).

E_{pa} (by 38 ± 1 mV) for SC_3Fc SAMs as compared to SC_4Fc SAMs. We note that Fc−Fc interactions dominate for the short SAMs ($n < 5$) because for thick SAMs with $n > 5$ C_n−C_n interactions dominate.[12,58]

Nanoscopic Characterization of the SAMs. To explore the packing structure of the SAMs at the nanoscale, we performed STM experiments at room temperature under UHV conditions (2.0×10^{-10} mbar). We have used electrochemically etched tungsten tips. We prepared the SAMs on hydrogen flame annealed Au(111) surfaces, after which we introduced the samples immediately into the high vacuum chamber of the STM in order to minimize contamination from the ambient as much as possible. Despite these precautions, we found that physisorbed materials were always present on our samples (bright dots on the surface in Figure 3B, for instance). Müller-Meskamp et al.[19] also reported the presence of excess molecules. As described above, annealing at 70 °C for 45 min reduced the amount of physisorbed materials.

Figure 3 shows the STM images of SAMs of SC_3Fc from which we make the following five observations. (i) The SAMs form well-ordered domains (Figure 3A−C). (ii) The angle between two orientations of stripes of neighboring domains, γ (see below), is ~74° (Figure 3A). (iii) The broad stripes (caused by row defects; see below) with a width of ~4 nm

Table 2. Unit Cells of SAMs of SC_3Fc and SC_4Fc on Au(111) Compared to the Unit Cells of Their Bulk Crystals in the *bc*-Plane

	SC_3Fc		SC_4Fc		
			SAMs		
	SAMs	bulk crystal	A	B	bulk crystal
unit cell of SAMs[a]	$2\sqrt{3}a \times 6a$		$4a \times 7a$	$\sqrt{31}a \times 2\sqrt{13}a$	
dimension (nm)[b]	1.73 × 2.07	1.53 × 2.58	1.66 × 2.08	1.15 × 2.02	1.73 × 2.02
α (deg)[c]	60.2°	61.55°	45.4°	45.4°	44.06°
γ (deg)[d]	~74°	90°	~60°	~80 °	90°
packing density[e] (molecule/nm^2)	2.3	2.0	2.0	1.2	1.2
surface coverage (molecule/nm^2)[f]	1.7		1.8	1.8	

[a] a is the 0.288 nm lattice parameter of Au(111). [b] Dimension is defined as width × length of the unit cell in nm. [c] α is the tilt angle of the Fc units. [d] γ is the angle between the edges of a unit cell. [e] See Supporting Information page S3 for details. [f] The surface coverage was obtained by CVs as explained in the main text.

dx.doi.org/10.1021/la503493x | *Langmuir* 2014, 30, 13447−13455

contain a perpendicularly orientated striped pattern with a width of ~0.4 nm (Figure 3B). (iv) The orientation of the pattern is retained in subsequent Au terraces (Figure 3C). (v) The line scans in panels 3D show that the apparent depth of the groove between the broad stripes is ~15 pm (Figure 3E).

Figure 4 shows STM images of well-ordered domains of SC_4Fc on Au(111). Two domains coexist. These coexisting

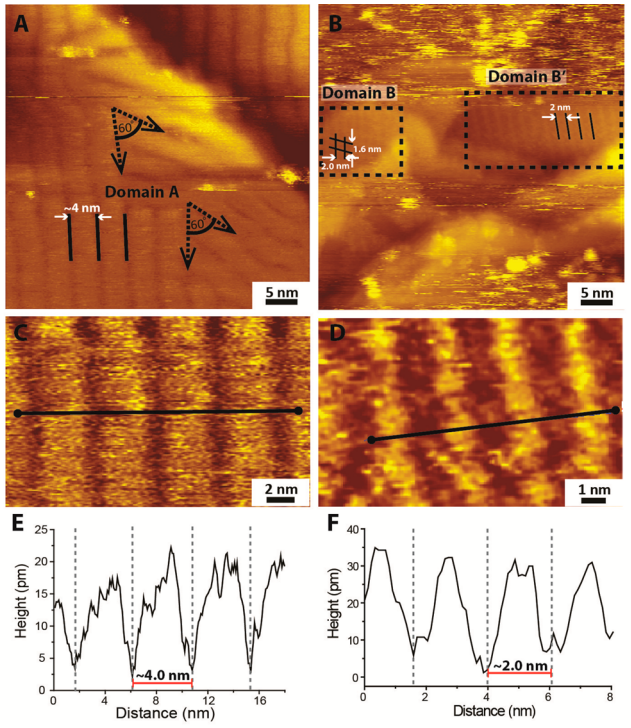

Figure 4. STM images of SAMs of SC_4Fc on Au(111). (A) Domain A consists of stripes with a width of ~4 nm. (B) Domain B with the intersecting of two striped patterns. The unit cell of domain B is 1.60 nm by 2.08 nm. The width of the stripes of domain B′ is 2.0 nm (as explained in the main text, we believe that domain B and B′ are the same). (C) Magnification of domain A. (D) Magnification of domain B′. STM height profiles of domain A (E) and B′ (F).

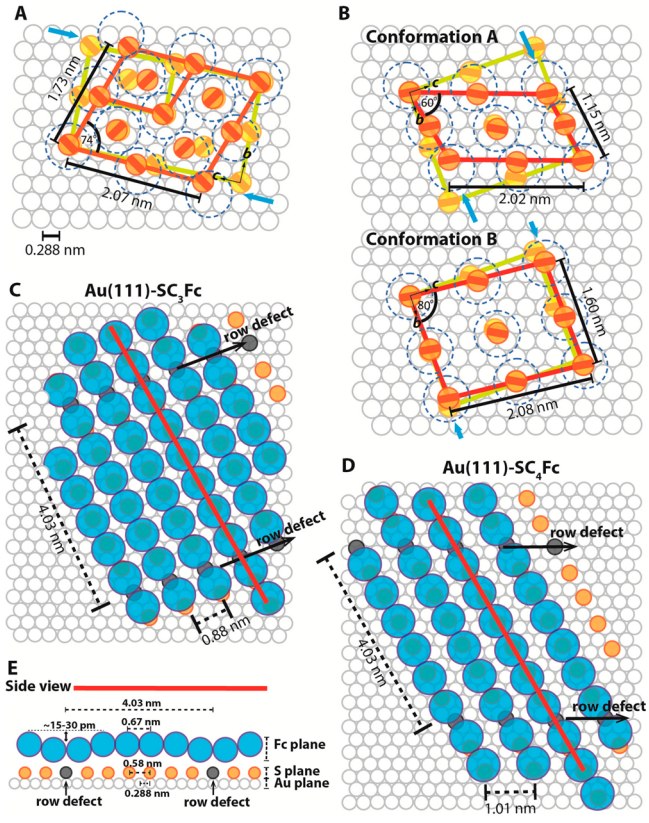

Figure 5. Proposed models for the SAMs of (A) SC_3Fc and (B) SC_4Fc on Au(111). Orange circles and parallelograms represent sulfur lattices and unit cells of the SAM, respectively. Yellow circles and parallelograms represent the sulfur lattices and unit cells of the bulk crystal on *bc*-plane placed on Au(111), respectively. Fc lattices of the SAMs of (C) SC_3Fc and (D) SC_4Fc on Au(111). (E) Side view of the SAMs packing of SC_3Fc and SC_4Fc, showing the mismatch in distance between sulfur atoms (0.58 nm) and between Fc units (0.67 nm). Blue and black circles represent Fc lattices and row defects, respectively, and diagonal lines in the circles represent the orientation of Fc units (perpendicular to Cp plane). Blue arrows represent the direction of lattice distortions with respect to crystal structure.

domains are labeled A and B/B′, respectively, as indicated in Figure 4A and B. Figure 4A shows the presence of broad stripes of ~4 nm with an γ of ~60° (domain A). Figure 4B shows the intersection of two stripes with different spacing of 1.6 × 2.0 nm with γ of ~80° (domain B), and stripes with a width of 2.0 nm aligned parallel to domain B′. Figure 4C and D shows a magnification of the pattern of domains A and B′. The apparent height profiles show that the grooves between the stripes of domain A (Figure 4E) and domain B′ (Figure 4F) have a depth of ~20 and ~30 pm, respectively. Domains B and B′ seem to be similar since both domains consist of the same width of vertical stripes (2.0 nm), but the horizontal line could not be observed for domain B′ due to low contrast in the STM image.

Packing of the SAMs. Here we propose unit cells of the SAMs based on lattice spacing obtained from the crystal structures of their corresponding thiol derivatives and the angular distortion of the γ values obtained from STM results (Figure 3 and 4). We report these unit cells in units of *a* which is the nearest-neighbor distance (0.288 nm) of gold atoms in Au(111). Figure 5 shows the models for the SAMs of SC_3Fc and SC_4Fc. Figure 5A shows the proposed sulfur lattice (orange circles) for SAMs of SC_3Fc on Au(111). The rectangular unit cell of the sulfur atoms of the molecules in the single crystal structure are given in yellow circles. It is well-known that the sulfurs of SAMs of SC_n on Au(111) pack in a $(\sqrt{3} \times \sqrt{3})$ $R30°$ lattice.[28,29] In our case, the lattice of the sulfurs on the surface (γ values) is distorted from 60° (expected from the $(\sqrt{3} \times \sqrt{3})$ $R30°$ lattice of Au) because of the large Fc terminal groups. These angular distortions of the γ values are similar to observations reported by Piorier et al.[59] for the packing of SAMs with bulky terminal group, that is, SC_6OH (γ = ~74°), and Jin et al.[60] for the SAMs of aromatic thiols, that is, thiopyridine and thiolphenol (γ = ~75−80°). We were not able to resolve the orientation of the Fc units from the STM images, and the diagonal lines in the circles represent the orientation of the Fc obtained from the crystal structures.

For SAMs of SC_3Fc, we propose a primitive unit cell $6a \times 2\sqrt{13}a$ with γ of 74° and dimensions of 2.07 × 1.73 nm. The sulfur lattice on Au(111) is stretched by 13% in the *b*-axis and compressed by 20% in the *c*-axis relative to those of the crystal structure of HSC_3Fc (Figure 5A). The deviations between *b*- and *c*-axis lead to the distorted angle of 74° as well as the buildup of strain between the Fc moieties. We believe that this strain causes the sulfurs to skip a row in order to release the

dx.doi.org/10.1021/la503493x | *Langmuir* 2014, 30, 13447−13455

strain at certain intervals (~4 nm, equal to 6 molecules), resulting in row defects and stripes (Figure 5C). Figure 5E shows the side view of the SC_3Fc SAM packing model and indicates the different spacing between the sulfur atoms (0.58 nm) and the Fc units (0.67 nm).[47] This figure shows that strain is relieved when the sulfurs skip one row every six molecules, resulting in a local depression. The depth of these depressions is 15−30 pm (see STM height profiles in Figures 3E for SC_3Fc and 4E,F for SC_4Fc).

For SAMs of SC_4Fc, we propose two models to explain the structures of domains A and B. For domain A, we propose a primitive unit cell with a dimension of $4a \times 7a$ with γ of 60° and dimensions of 1.15 × 2.02 nm (Figure 5B conformation A). The lattice of the sulfurs is distorted from that derived from the crystal structure of HSC_4Fc by a relatively large compression of the *b*-axis of 34% and only by stretching the *c*-axis by 3%. This distortion of *b*-axis results in the buildup of strain and induces row defects at intervals of 2.08 nm observed as "stripes" (or grooves) in the STM images (Figure 4) as described above.

The proposed unit cell for domain B is $\sqrt{13}a \times 2\sqrt{13}a$ with γ of 80° and dimensions of 1.60 × 2.08 nm (Figure 5B conformation B). The lattice of the sulfurs is only slightly distorted relative to that of the crystal structure by 8% compression in the *b*-axis and 3% stretch in the *c*-axis. These small distortions explain the absence of the defect rows (or grooves) in conformation B (because no strain builds up relative to the crystal structure). We believe that the stripes that are visible in the STM image (Figure 4B) represent the dimension of the units because the stripes have a spacing of 2.0 nm and the 1.6 nm spacing in the *b*-direction. The small height difference between two stripes (~30 pm; Figure 4F) could be caused by different Fc orientations because of a difference in the twist angle β[13] between rows of molecules (as is also observed in the crystal structure), but we were not able to resolve these subtle molecular effects from the STM images.

All proposed unit cells are parallelograms. For SAMs of SC_3Fc, the $6a \times 2\sqrt{13}a$ unit cell occupies an area of 3.44 nm^2 with eight molecules, resulting in a packing density of 2.33 molecule/nm^2. For SAMs of SC_4Fc in conformation A, the $4a \times 7a$ unit cell occupies an area of 2.01 nm^2 with four molecules, resulting in a packing density of 1.99 molecule/nm^2. For SAMs of SC_4Fc in conformation B, the $\sqrt{13}a \times 2\sqrt{13}a$ unit cell occupies an area of 3.28 nm^2 with four molecules, resulting in a packing density of 1.22 molecule/nm^2. These numbers agree well with a packing density of ~2 molecule/nm^2 (or ~3.0 × 10^{-10} mol/cm^2) obtained experimentally by CVs for SAMs of SC_3Fc and SC_4Fc. These surface coverages are about 30% lower than the packing density of SC_nFc SAMs with $n > 5$ (2.7 molecule/nm^2, or 4.5 × 10^{-10} mol/cm^2) based on a simple hexagonal packing model for Fc units where the Fc units are treated as spheres with a diameter of 0.67 nm.[9] As mentioned above, these SAMs are dominated by C_n−C_n interactions and not by Fc−Fc interactions when $n < 5$.[12,58] Figure 6 shows the α and β values of the Fc units for the proposed unit cells. The α values are 60° and 45° (in agreement with the NEXAFS data) for SAMs of SC_3Fc and SC_4Fc, respectively, with a twist angle β of 0° and 90° between rows of molecules (for example, between rows I and II) based on the XRD data. As a result, the Fc units are orientated EF for the SC_3Fc SAMs and FF for the SC_4Fc SAMs, which explains the patterns observed in the STM image.

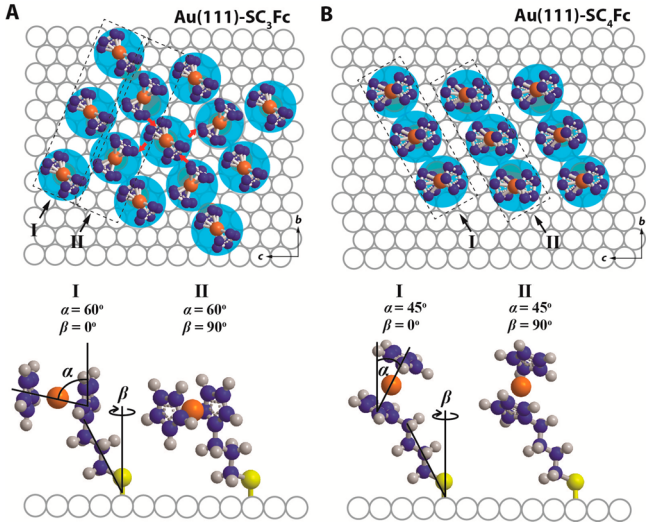

Figure 6. Top and side views of the proposed models of the orientation of the Fc moieties of SAMs of (A) SC_3Fc and (B) SC_4Fc. The schematic of the top view shows that the Fc groups of the SC_3Fc SAM pack edge-to-face (red arrows), while the Fc groups of the SC_4Fc SAM aligns more upright in a parallel orientation. The side views show the α value for SC_nFc SAMs with $n = 3$ is larger than that for $n = 4$ (in agreement with NEXAFS) and the difference in value of β between neighboring molecules indicated by I and II (in agreement with XRD).

CONCLUSIONS

We have imaged ordered domains of SAMs of SC_3Fc and SC_4Fc by STM. The STM imaging was made possible after annealing up to 70 °C to remove physisorbed materials. Our HREELS results indicate that annealing did not induce phase transitions or damage the SAMs. We studied the supramolecular structure of the SAMs using techniques that probe large areas (HREELS, CV, and NEXAFS) which are complementary to scanning probe based techniques. The agreement between all these techniques shows that the STM images represent the structures of the SAMs very well. The proposed unit cells of the SAMs are similar to that of the crystal structures but are distorted. The distortions are induced by the mismatch in size between the Fc (0.67 nm) units and the sulfur atoms (0.58 nm), which cause the buildup of strain in the SAMs. This strain is relieved when the sulfurs skip one row on the Au(111) surface, which were observed as stripes at regular intervals of six molecules for the SC_3Fc and SC_4Fc SAM, respectively.

We propose that the SAMs pack into the following unit cells: $6a \times 2\sqrt{13}a$ with γ of 74° for SAMs of SC_3Fc, and $4a \times 7a$ with γ of 60° (conformation A) and $\sqrt{13}a \times 2\sqrt{13}a$ with γ of 80° (conformation B) for SAMs of SC_4Fc, which are essentially distorted crystal packing structures. The molecules are standing up (despite the short alkyl chains), and the α values of the Fc units are determined by the number of CH_2 units (because the Au−S−C bond angle is fixed). Thus, the outcome of the assembly process is governed by odd−even effects, intermolecular interactions, and the buildup of lattice strain due to the mismatch in size of the bulky terminal Fc groups and the sulfur anchoring groups. Our findings improve our understanding of the supramolecular structure of these SAMs, but we believe that the findings reported here also apply to other systems.

dx.doi.org/10.1021/la503493x | *Langmuir* 2014, 30, 13447−13455

■ ASSOCIATED CONTENT

Supporting Information

Experimental details of fabrication of Au substrates, X-ray single crystal diffraction, and crystal data and structure refinement for HSC_3Fc and HSC_4Fc. This material is available free of charge via the Internet at http://pubs.acs.org.

■ AUTHOR INFORMATION

Corresponding Author

*E-mail: Christian.nijhuis@nus.edu.sg.

Notes

The authors declare no competing financial interest.

■ ACKNOWLEDGMENTS

The Singapore National Research Foundation (NRF Award No. NRF-RF2010-03 to C.A.N.) is kindly acknowledged for supporting this research.

■ REFERENCES

(1) Halik, M.; Hirsch, A. The Potential of Molecular Self-Assembled Monolayers in Organic Electronic Devices. *Adv. Mater.* **2011**, *23*, 2689−2695.

(2) Dubi, Y. Transport through Self-Assembled Monolayer Molecular Junctions: Role of In-Plane Dephasing. *J. Phys. Chem. C* **2014**, *118*, 21119−21127.

(3) Wang, Q.; Evans, N.; Zakeeruddin, S. M.; Exnar, I.; Grätzel, M. Molecular Wiring of Insulators: Charging and Discharging Electrode Materials for High-Energy Lithium-Ion Batteries by Molecular Charge Transport Layers. *J. Am. Chem. Soc.* **2007**, *129*, 3163−3167.

(4) Knesting, K. M.; Hotchkiss, P. J.; MacLeod, B. A.; Marder, S. R.; Ginger, D. S. Spatially Modulating Interfacial Properties of Transparent Conductive Oxides: Patterning Work Function with Phosphonic Acid Self-Assembled Monolayers. *Adv. Mater.* **2012**, *24*, 642−646.

(5) Wilson, G. S.; Armstrong, F. A. Recent Developments in Faradaic Bioelectrochemistry. *Electrochim. Acta* **2000**, *45*, 2623−2645.

(6) Li, C.; Liu, M.; Pschirer, N. G.; Baumgarten, M.; Müllen, K. Polyphenylene-Based Materials for Organic Photovoltaics. *Chem. Rev.* **2010**, *110*, 6817−6855.

(7) Cheng, X. Y.; Noh, Y. Y.; Wang, J. P.; Tello, M.; Frisch, J.; Blum, R. P.; Vollmer, A.; Rabe, J. P.; Koch, N.; Sirringhaus, H. Controlling Electron and Hole Charge Injection in Ambipolar Organic Field-Effect Transistors by Self-Assembled Monolayers. *Adv. Funct. Mater.* **2009**, *19*, 2407−2415.

(8) Eckermann, A. L.; Feld, D. J.; Shaw, G. A.; Meade, T. J. Electrochemistry of Redox-Active Self-Assembled Monolayers. *Coord. Chem. Rev.* **2010**, *254*, 1769−1802.

(9) Chidsey, C. E. D.; Bertozzi, C. R.; Putvinski, T. M.; Mujsce, A. M. Coadsorption of Ferrocene-Terminated and Unsubstituted Alkanethiols on Gold: Electroactive Self-Assembled Monolayers. *J. Am. Chem. Soc.* **1990**, *112*, 4301−4306.

(10) Creager, S. E.; Rowe, G. K. Redox Properties of Ferrocenylalkane Thiols Coadsorbed with Linear Normal-Alkanethiols on Polycrystalline Bulk Gold Electrodes. *Anal. Chim. Acta* **1991**, *246*, 233−239.

(11) Uosaki, K.; Sato, Y.; Kita, H. Electrochemical Characteristics of a Gold Electrode Modified with a Self-Assembled Monolayer of Ferrocenylalkanethiols. *Langmuir* **1991**, *7*, 1510−1514.

(12) Nerngchamnong, N.; Yuan, L.; Qi, D. C.; Li, J.; Thompson, D.; Nijhuis, C. A. The Role of Van Der Waals Forces in the Performance of Molecular Diodes. *Nat. Nanotechnol.* **2013**, *8*, 113−118.

(13) Tao, F.; Bernasek, S. L. Understanding Odd-Even Effects in Organic Self-Assembled Monolayers. *Chem. Rev.* **2007**, *107*, 1408−1453.

(14) Poirier, G. E. Characterization of Organosulfur Molecular Monolayers on Au(111) Using Scanning Tunneling Microscopy. *Chem. Rev.* **1997**, *97*, 1117−1127.

(15) Chiang, S. Scanning Tunneling Microscopy Imaging of Small Adsorbed Molecules on Metal Surfaces in an Ultrahigh Vacuum Environment. *Chem. Rev.* **1997**, *97*, 1083−1096.

(16) Wu, H.; Sotthewes, K.; Kumar, A.; Vancso, G. J.; Schon, P. M.; Zandvliet, H. J. W. Dynamics of Decanethiol Self-Assembled Monolayers on Au(111) Studied by Time-Resolved Scanning Tunneling Microscopy. *Langmuir* **2013**, *29*, 2250−2257.

(17) Sotthewes, K.; Wu, H.; Kumar, A.; Vancso, G. J.; Schon, P. M.; Zandvliet, H. J. W. Molecular Dynamics and Energy Landscape of Decanethiolates in Self-Assembled Monolayers on Au(111) Studied by Scanning Tunneling Microscopy. *Langmuir* **2013**, *29*, 3662−3667.

(18) Hobara, D.; Ota, M.; Imabayashi, S.; Niki, K.; Kakiuchi, T. Phase Separation of Binary Self-Assembled Thiol Monolayers Composed of 1-Hexadecanethiol and 3-Mercaptopropionic Acid on Au(111) Studied by Scanning Tunneling Microscopy and Cyclic Voltammetry. *J. Electroanal. Chem.* **1998**, *444*, 113−119.

(19) Müller-Meskamp, L.; Karthauser, S.; Waser, R.; Homberger, M.; Wang, Y.; Englert, U.; Simon, U. Structural Ordering of Omega-Ferrocenylalkanethiol Monolayers on Au(111) Studied by Scanning Tunneling Microscopy. *Surf. Sci.* **2009**, *603*, 716−722.

(20) Tucker, E. Z.; Gorman, C. B. Terminal Alkynes as an Ink or Background SAM in Replacement Lithography: Adventitious versus Directed Replacement. *Langmuir* **2010**, *26*, 15027−15034.

(21) Dionne, E. R.; Sultana, T.; Norman, L. L.; Toader, V.; Badia, A. Redox-Induced Ion Pairing of Anionic Surfactants with Ferrocene-Terminated Self-Assembled Monolayers: Faradaic Electrochemistry and Surfactant Aggregation at the Monolayer/Liquid Interface. *J. Am. Chem. Soc.* **2013**, *135*, 17457−17468.

(22) Zhu, H.; Hacker, C. A.; Pookpanratana, S. J.; Richter, C. A.; Yuan, H.; Li, H.; Kirillov, O.; Loannou, D. E.; Li, Q. Non-Volatile Memory with Self-Assembled Ferrocene Charge Trapping Layer. *Appl. Phys. Lett.* **2013**, *103*, 053102.

(23) Li, Z.; Liu, Y.; Mertens, S. F. L.; Pobelov, I. V.; Wandlowski, T. From Redox Gating to Quantized Charging. *J. Am. Chem. Soc.* **2010**, *132*, 8187−8193.

(24) Nijhuis, C. A.; Reus, W. F.; Whitesides, G. M. Molecular Rectification in Metal-SAM-Metal Oxide-Metal Junctions. *J. Am. Chem. Soc.* **2009**, *131*, 17814−17827.

(25) Reus, W. F.; Thuo, M. M.; Shapiro, N. D.; Nijhuis, C. A.; Whitesides, G. M. The SAM, Not the Electrodes, Dominates Charge Transport in Metal-Monolayer//Ga_2O_3/Gallium-Indium Eutectic Junctions. *ACS Nano* **2012**, *6*, 4806−4822.

(26) Ulman, A. Formation and Structure of Self-Assembled Monolayers. *Chem. Rev.* **1996**, *96*, 1533−1554.

(27) Love, J. C.; Estroff, L. A.; Kriebel, J. K.; Nuzzo, R. G.; Whitesides, G. M. Self-Assembled Monolayers of Thiolates on Metals as a Form of Nanotechnology. *Chem. Rev.* **2005**, 1103−1169.

(28) Poirier, G. E.; Tarlov, M. J. The c(4×2) Superlattice of *n*-Alkanethiol Monolayers Self-Assembled on Au(111). *Langmuir* **1994**, *10*, 2853−2856.

(29) Fenter, P.; Eberhardt, A.; Eisenberger, P. Self-Assembly of *n*-Alkyl Thiols as Disulfides on Au(111). *Science* **1994**, *266*, 1216−1218.

(30) Wolf, H.; Ringsdorf, H.; Delamarche, E.; Takami, T.; Kang, H.; Michel, B.; Gerber, C.; Jaschke, M.; Butt, H. J.; Bamberg, E. End Group Dominated Molecular Order in Self-Assembled Monolayers. *J. Phys. Chem.* **1995**, *99*, 7102−7107.

(31) Müller-Meskamp, L.; Karthauser, S.; Waser, R.; Homberger, M.; Simon, U. Striped Phase of Mercaptoalkylferrocenes on Au(111) with a Potential for Nanoscale Surface Patterning. *Langmuir* **2008**, *24*, 4577−4580.

(32) Yokota, Y.; Fukui, K.; Enoki, T.; Hara, M. Origin of Current Enhancement Through a Ferrocenylundecanethiol Island Embedded in Alkanethiol SAMs by Using Electrochemical Potential Control. *J. Phys. Chem. C* **2007**, *111*, 7561−7564.

(33) Fujii, S.; Kurokawa, S.; Murase, K.; Lee, K. H.; Sakai, A.; Sugimura, H. Self-Assembled Mixed Monolayer Containing Ferroce-

nylthiol Molecules: STM Observations and Electrochemical Investigations. *Electrochim. Acta* **2007**, *52*, 4436−4442.
(34) Wedeking, K.; Mu, Z.; Kehr, G.; Frohlich, R.; Erker, G.; Chi, L.; Fuchs, H. Tetradecylferrocene: Ordered Molecular Array of an Organometallic Amphiphile in the Crystal and in a Two-Dimensional Assembled Structure on a Surface. *Langmuir* **2006**, *22*, 3161−3165.
(35) Qune, L. F. N. A.; Tamada, K. Self-Assembling Properties of 11-Ferrocenyl-1-Undecanethiol on Highly Oriented Pyrolitic Graphite Characterized by Scanning Tunneling Microscopy. *e-J. Surf. Sci. Nanotechnol.* **2008**, *6*, 119−123.
(36) Rudnev, A. V.; Pobelow, I. V.; Wandlowski, T. Structural Aspects of Redox-Mediated Electron Tunneling. *J. Electroanal. Chem.* **2011**, *660*, 302−308.
(37) Viana, A. S.; Jones, A. H.; Abrantes, L. M.; Kalaji, M. Redox Induced Orientational Changes in a Series of Short Chain Ferrocenyl Alkyl Thiols Self-Assembled on Gold(111) Electrodes. *J. Electroanal. Chem.* **2001**, *500*, 290−298.
(38) Riposan, A.; Liu, G.-Y. Significance of Local Density of States in the Scanning Tunneling Microscopy Imaging of Alkanethiol Self-Assembled Monolayers. *J. Phys. Chem. B* **2006**, *110*, 23926−23937.
(39) Qian, Y. L.; Yang, G. H.; Yu, J.; Jung, T. A.; Liu, G.-Y. Structures of Annealed Decanethiol Self-Assembled Monolayers on Au(111): an Ultrahigh Vacuum Scanning Tunneling Microscopy Study. *Langmuir* **2003**, *19*, 6056−6065.
(40) Nuzzo, R. G.; Zegarski, B. R.; Dubois, L. H. Fundamental Studies of the Chemisorption of Organosulfur Compounds on Au(111): Implications for Molecular Self-Assembly on Gold Surfaces. *J. Am. Chem. Soc.* **1987**, *100*, 733−740.
(41) Weiss, E. A.; Chiechi, R. C.; Kaufman, G. K.; Kriebel, J. K.; Li, Z.; Duati, M.; Rampi, M. A.; Whitesides, G. M. Influence of Defects on the Electrical Characteristics of Mercury-Drop Junctions: Self-Assembled Monolayers of *n*-Alkanethiolates on Rough and Smooth Silver. *J. Am. Chem. Soc.* **2007**, *129*, 4336−4349.
(42) Creager, S. E.; Rowe, G. K. Competitive Self-Assembly and Electrochemistry of some Ferrocenyl-*n*-Alkanethiol Derivatives on Gold. *J. Electroanal. Chem.* **1994**, *370*, 203−211.
(43) Sheldrick, G. M. A Short History of SHELX. *Acta Crystallogr.* **2008**, *64*, 112−122.
(44) Delamarche, E.; Michel, B.; Kang, H.; Gerber, C. Thermal Stability of Self-Assembled Monolayers. *Langmuir* **1994**, *10*, 4103−4108.
(45) Durston, P. J.; Palmer, R. E. Adsorption and Decomposition of Ferrocene on Graphite Studied by HREELS and STM. *Surf. Sci.* **1998**, *400*, 277−280.
(46) Woodbridge, C. M.; Pugmire, D. L.; Johnson, R. C.; Boag, N. M.; Langell, M. A. HREELS and XPS Studies of Ferrocene on Ag(100). *J. Phys. Chem. B* **2000**, *104*, 3085−3093.
(47) Waldfried, C.; Welipitiya, D.; Hutchings, C. W.; de Silva, H. S. V.; Gallup, G. A.; Dowben, P. A.; Pai, W. W.; Zhang, J. D.; Wendelken, J. F.; Boag, N. M. Preferential Bonding Orientations of Ferrocene on Surfaces. *J. Phys. Chem. B* **1997**, *101*, 9782−9789.
(48) Connelly, N. G.; Geiger, W. E. Chemical Redox Agents for Organometallic Chemistry. *Chem. Rev.* **1996**, *96*, 877−910.
(49) Laviron, E. Surface Linear Potential Sweep Voltammetry: Equation of Peaks for a Reversible-Reaction when Interactions between Adsorbed Molecules are Taken into Account. *J. Electroanal. Chem.* **1974**, *52*, 395−402.
(50) Rühl, E.; Heinzel, C.; Baumgärtel, H.; Hitchcock, A. P. Ionic Fragmentation of Carbon 1s Excited Metallocenes. *Chem. Phys.* **1993**, *169*, 243−257.
(51) Watcharinyanon, S.; Moons, E.; Johansson, L. S. O. Mixed Self-Assembled Monolayers of Ferrocene-Terminated and Unsubstituted Alkanethiols on Gold: Surface Structure and Work Function. *J. Phys. Chem. C* **2009**, *113*, 1972−1979.
(52) Otero, E.; Kosugi, N.; Urquhart, S. G. Strong Double Excitation and Open-Shell Features in the Near-Edge X-Ray Absorption Fine Structure Spectroscopy of Ferrocene and Ferrocenium Compounds. *J. Chem. Phys.* **2009**, *131*, 114313.
(53) Ye, S.; Sato, Y.; Uosaki, K. Redox-Induced Orientation Change of a Self-Assembled Monolayer of 11-Ferrocenyl-1-Undecanethiol on a Gold Electrode Studied by in Situ FT-IRRAS. *Langmuir* **1997**, *13*, 3157−3161.
(54) Macrae, C. F.; Bruno, I. J.; Chisholm, J. A.; Edgington, P. R.; Mccabe, P.; Pidcock, E.; Rodriguez-Monge, L.; Taylor, R.; van de Streek, J.; Wood, P. A. Mercury CSD 2.0: New Features for the Visualization and Investigation of Crystal Structures. *J. Appl. Crystallogr.* **2008**, *41*, 466−470.
(55) Cao, L.; Li, Y.; Qi, D.-C.; Nerngchamnong, N.; Thompson, D.; Hamoudi, H.; Wee, A. T. S.; Nijhuis, C. A. Manuscript in preparation.
(56) Braga, D.; Grepioni, F. Crystal Construction and Molecular Interplay in Solid Ferrocene, Nickelocene, and Ruthenocene. *Organometalllics* **1992**, *11*, 711−718.
(57) Dunitz, J. D. Phase Changes and Chemical Reactions in Molecular Crystals. *Acta Crystallogr.* **1995**, *51*, 619−631.
(58) Nerngchamnong, N.; Thompson, D.; Cao, L.; Yuan, L.; Jiang, L.; Roemer, M.; Nijhuis, C. A. Manuscript in preparation.
(59) Poirier, G. E.; Pylant, E. D.; White, J. M. Crystalline Structures of Pristine and Hydrated Mercaptohexanol Self-Assembled Monolayers on Au(111). *J. Chem. Phys.* **1996**, *105*, 2089−2092.
(60) Jin, Q.; Rodriguez, J. A.; Li, C. Z.; Darici, Y.; Tao, N. J. Self-Assembly of Aromatic Thiols on Au(111). *Surf. Sci.* **1999**, *425*, 101−111.